



# CHORUS

This is the accepted manuscript made available via CHORUS. The article has been published as:

## Electronic structure of $\text{CuTeO}_4$ and its relationship to cuprates

Antia S. Botana and Michael R. Norman

Phys. Rev. B **95**, 115123 — Published 13 March 2017

DOI: [10.1103/PhysRevB.95.115123](https://doi.org/10.1103/PhysRevB.95.115123)

# Electronic structure of $\text{CuTeO}_4$ and its relationship to cuprates

Antia S. Botana<sup>1</sup> and Michael R. Norman<sup>1</sup>

<sup>1</sup>*Materials Science Division, Argonne National Laboratory, Argonne, Illinois 60439, USA*

Based on first principles calculations, the electronic structure of  $\text{CuTeO}_4$  is discussed in the context of superconducting cuprates. Despite some significant crystallographic differences, we find that  $\text{CuTeO}_4$  is similar to these cuprates, exhibiting a quasi two dimensional electronic structure that involves hybridized Cu-*d* and O-*p* states in the vicinity of the Fermi level, along with an antiferromagnetic insulating ground state. Hole doping this material by substituting  $\text{Te}^{6+}$  with  $\text{Sb}^{5+}$  would be of significant interest.

High-temperature superconductivity in cuprates is one of the most intriguing emergent phenomena in strongly correlated electron systems [1]. Some common features of cuprates include their layered crystal structures, proximity to a magnetic insulating state, and hybridization of Cu-*d* and O-*p* orbitals. The investigation of materials with features in common with these is key to establish the importance of these various features for superconductivity and to provide guidance in the search for new high temperature superconductors.

In spite of an intense search for new cuprates, copper tellurates [2] have not been explored for potential superconductivity. A number have been reported in regards to their crystal structures. Those where Cu is 2+ and Te is 6+ include  $\text{CuTeO}_4$  [3],  $\text{Cu}_3\text{TeO}_6$  [4],  $\text{Sr}_2\text{CuTeO}_6$  [5] (and its Ba variant [6]),  $\text{Ag}_4\text{CuTeO}_6$ , [7], and  $\text{Na}_2\text{Cu}_2\text{TeO}_6$  [8]. Several also exist where Te can be in a 4+ state ( $\text{CuTe}_2\text{O}_5$ ,  $\text{PbCuTe}_2\text{O}_6$ ,  $\text{SrCuTe}_2\text{O}_7$ ) that we do not discuss here. Some of these materials have been investigated for their interesting magnetic properties, but in all these cases, their crystal structures do not resemble those of cuprates.  $\text{Ag}_4\text{CuTeO}_6$  and  $\text{Na}_2\text{Cu}_2\text{TeO}_6$  have Cu-O-Te-O-Cu chains,  $\text{Cu}_3\text{TeO}_6$  has a 3D array of Cu hexagons, and though  $\text{Sr}_2\text{CuTeO}_6$  exhibits a square planar net, the Cu ions are connected by a superexchange pathway (Cu-O-Te-O-Cu) as in the chain materials. The exception is  $\text{CuTeO}_4$ , which is the focus of this Letter.

Even though its crystal structure was reported almost forty years ago [3], the electronic and magnetic properties of  $\text{CuTeO}_4$  have not been explored. This may be due to the difficulty of growing the material ( $\text{Cu}_3\text{TeO}_6$  tends to form instead [9]), and the fact that the crystals are disordered, probably due to stacking faults. On the other hand, unlike the above mentioned materials,  $\text{CuTeO}_4$  exhibits  $\text{CuO}_2$  planes, though they are highly buckled (Fig. 1). This occurs because, unlike in most cuprates, the copper ions are in a distorted octahedral environment with Cu-O bond lengths varying by less than 20%.

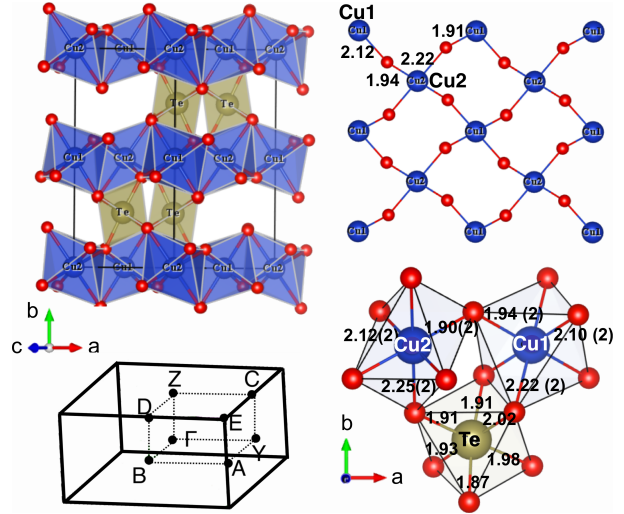


FIG. 1. Crystal structure of  $\text{CuTeO}_4$  illustrating the buckled  $\text{CuO}_2$  planes (upper right) that result from coupling of  $\text{CuO}_6$  octahedra to  $\text{TeO}_6$  octahedra (upper left). Also shown is the corresponding Brillouin zone with high symmetry points marked (lower left), as well as the local environment of the Cu and Te ions (lower right) Note that the orthorhombic zone has axes that are rotated  $45^\circ$  relative to a tetragonal cuprate.

Moreover, the planes are coupled by  $\text{TeO}_6$  octahedra which share oxygen atoms with the  $\text{CuO}_6$  octahedra, driving the strong buckling with the ‘planar’ Cu-O bonds tilted from  $24.1^\circ$  to  $28.4^\circ$  out of the plane. Regardless, our electronic structure calculations show considerable similarities of this material to the superconducting cuprates, though with some interesting differences.

Electronic structure calculations were performed within density functional theory [10, 11] using the all-electron, full potential code WIEN2k [12] based on an augmented plane wave plus local orbitals (APW+lo) basis set [13]. We have used the Perdew-Burke-Ernzerhof version of the generalized gradient approximation (PBE-GGA) for the exchange-correlation potential [14]. Calculations including spin-orbit coupling are shown in Ref. 15. The pa-

parameters used were  $R_{mt}K_{max}=7.0$ , with muffin-tin radii of 1.93 for Cu, 1.89 for Te, and 1.63 for O (a.u.). Brillouin zone integrations were done with a  $10\times 16\times 5$  mesh. We performed calculations both with the experimental structural parameters taken from Falck *et al.* [3] and with fully relaxed atomic positions.

Though the crystals are disordered, Falck *et al.* [3] report a monoclinic structure with  $P2_1/n$  symmetry.  $\text{CuTeO}_4$  has 4 formula units per unit cell ( $Z=4$ ) containing two inequivalent Cu sites, four inequivalent oxygens and one Te site. As mentioned above, the Cu ions exhibit a highly distorted octahedral environment with 2 short, 2 medium and 2 long Cu-O distances ranging from 1.91 to 2.26 Å for Cu1 and 1.94 to 2.22 Å for Cu2 (Fig. 1 and Table I). The  $\text{CuO}_2$  planes are not as regular as in a typical cuprate, with alternating Cu1 and Cu2 ions, and Cu-O-Cu bond angles of  $122.5^\circ$  or  $126.1^\circ$  along nearly orthogonal directions ( $81.1^\circ$  and  $98.9^\circ$ ). It should be noted that the Cu2-O long bonds lie within the buckled planes (Fig. 1). The  $\text{TeO}_6$  octahedra are less distorted, with Te-O distances ranging from 1.87 to 2.02 Å. The oxygens in the  $\text{CuO}_2$  planes are shared by the Te ions causing the buckling of these planes. The structural relaxation performed within GGA-PBE (Table I) tends to reduce the octahedral distortion by nearly balancing the short and medium Cu-O distances. This tendency points towards the possibility that the reported short-medium-long pattern of the Cu-O bonds can be due to a dynamic Jahn-Teller effect [16] since the structure was determined at room temperature. Detailed measurements of the structure and its atomic displacement parameters as a function of temperature could shed light on this.

Assuming a completely ionic character, Cu would be in a  $2+$  state ( $d^9$ ). The paramagnetic band structure, which is metallic because of the odd number of electrons per cell, is shown in Fig. 2 along several high symmetry directions in the Brillouin zone as well as the corresponding density of states (DOS).

The Cu- $3d$  and O- $2p$  states form a complex of hybridized valence bands with a total bandwidth of  $\sim 9$  eV. In spite of the complexity of the valence-band manifold, the band structure around  $E_F$  is rather simple with four bands crossing the Fermi level. With the  $t_{2g}$  states being fully occupied for the Cu atoms, these bands have contributions from both Cu1 and Cu2 and are an admixture of  $d_{x^2-y^2}$  and  $d_{z^2}$ -like states (due to the 2-2-2 nature of the Cu-O bond lengths) with strong O- $2p$  hybridization. The strong hybridization between these states is evident given the similar shapes of the O and Cu DOS in the vicinity of the Fermi level more evident for

TABLE I. Cu-O and Te-O distances in the relaxed and unrelaxed structures. Note the different environments for the two inequivalent Cu sites. L, M, and S are used to specify the long, medium and short Cu-O bonds.

unrelaxed						
	O1 (L)	O3 (M)	O4 (S)			
Cu1	2.26	2.26	2.12	2.12	1.91	1.91
	O4 (L)	O2 (M)	O3 (S)			
Cu2	2.22	2.22	2.11	2.11	1.94	1.94
	O4	O3	O1	O2	O1	O2
Te	1.87	1.91	1.91	1.93	1.98	2.02
relaxed						
	O1	O1	O3	O3	O4	O4
Cu1	2.22	2.22	2.01	2.01	1.98	1.98
	O4	O4	O2	O2	O3	O3
Cu2	2.22	2.22	2.03	2.03	1.93	1.93
	O4	O3	O1	O2	O1	O2
Te	1.90	1.93	1.94	1.97	1.99	2.02

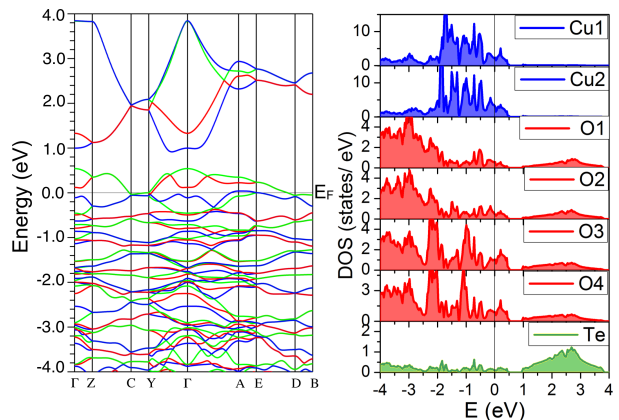


FIG. 2. Left: Paramagnetic band structure of  $\text{CuTeO}_4$  for the experimental structural data. Four Cu  $d$  - O  $p$  hybridized bands cross the Fermi level. Right: Atom resolved density of states for the Cu, O and Te ions.

O3 and O4 (the ‘planar’ oxygens) than for O1 and O2. The wide bands appearing above 2 eV correspond mainly to Te- $5s$  states hybridized with O- $2p$  states. There is no significant contribution of Te states around the Fermi level, pointing towards the quasi-two dimensionality of the electronic structure.

Turning to the band structure, the dispersion perpendicular to the  $\text{CuO}_2$  planes is small along certain zone directions ( $C$ - $Y$ ) but not as small along others ( $\Gamma$ - $Z$ ). The latter is characteristic of zone folding ( $Z=4$ ), with the absence of splitting at  $Z$  due to band sticking from the screw axis. Folding is also seen along in-plane directions, which is clearest along  $Z$ - $C$ , with the splitting being very small at  $C$  (0.02 eV). More complicated behavior is seen along  $\Gamma$ - $Y$

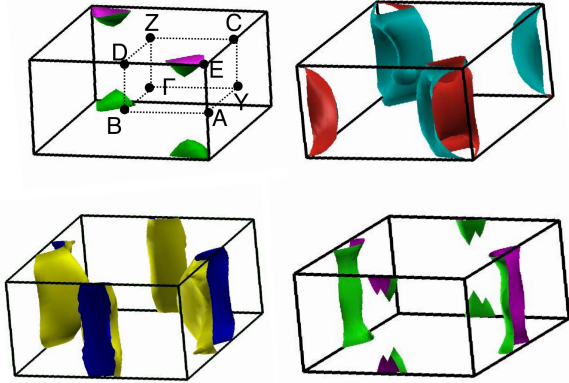


FIG. 3. The Fermi surfaces for  $\text{CuTeO}_4$  from the four bands in the paramagnetic state (top: hole-like bands; bottom: electron-like bands).

for two of the four bands due to their differing coupling along the  $b$  direction orthogonal to the planes. In this context, note that Cu1 and Cu2 atoms are related by  $(1/2, 0, 1/2)$  and  $(0, 1/2, 0)$  translations, and again all bands in the  $Z$ - $C$ - $E$ - $D$  zone face are doubly degenerate due to the screw axis.

The symmetries mentioned above are also reflected in the Fermi surfaces. For a typical cuprate, one finds warped cylinders. This is reminiscent of  $\text{CuTeO}_4$  where one of the hole surfaces is nearly cylindrical, centered at the zone corners ( $A$ - $E$ ), and two of the electron ones also nearly cylindrical, centered instead at the midline of the zone faces ( $A$ - $E$ - $D$ - $B$  and  $A$ - $E$ - $C$ - $Y$ ), with the electron and hole bands due to zone folding as in orthorhombic  $\text{La}_2\text{CuO}_4$  [17]. The remaining Fermi surfaces show a strong orthorhombic distortion, coupled with a more 3D-like behavior.

Given the magnetic character of the  $d^9$  ion, one might expect the paramagnetic state to be susceptible to magnetic order. We indeed find this to be the case, with the energy of the antiferromagnetic (AFM) state (with oppositely oriented spins on the Cu1 and Cu2 ions) being lower than that for the paramagnetic state by 34 meV/formula unit, and more stable than ferromagnetic ordering by 35 meV/formula unit. The corresponding band structure for the AFM state is shown in Fig. 4 and the atom-resolved DOS in Fig. 5. A small gap of  $\sim 0.13$  eV opens up due to the magnetic ordering, even without a Coulomb  $U$ , yielding a  $S=1/2$  AFM insulator. The gap becomes larger once a  $U$  is included as shown in Ref. 15. The gap is formed between minority-spin states only given that

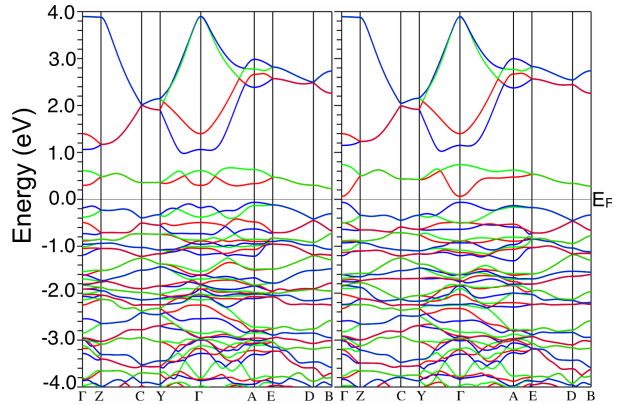


FIG. 4. Band structure of antiferromagnetic (AFM)  $\text{CuTeO}_4$  for the experimental structural data for the two spin channels (left: down; right: up). A small gap of 0.13 eV is apparent.

the crystal field splitting between the two  $e_g$  orbitals is smaller than the Hund's rule coupling. The two  $\text{Cu}^{2+}$ :  $d^9$  ( $S=1/2$ ) ions have one hole in the minority-spin  $d_{x^2-y^2}$ -like band with the highest occupied  $d$  states showing predominantly  $d_{z^2}$  character (with  $z$  being set along the long Cu-O bond for each Cu). The in plane AFM coupling reduces the admixture between  $d_{z^2}$  and  $d_{x^2-y^2}$  states with respect to the non magnetic case.

The slight differences in the band structure for up and down spin channels are due to the different environments of Cu1 and Cu2. The magnetic moments for the Cu atoms are  $\mu_{\text{Cu1}} = -0.53 \mu_B$  and  $\mu_{\text{Cu2}} = 0.52 \mu_B$ , reduced with respect to the nominal  $1 \mu_B$  value due to hybridization. Hybridization between the Cu- $d$  and O- $p$  states along with the low site symmetries for the oxygens induces small moments on the oxygen ions:  $\mu_{\text{O1}} = -0.01 \mu_B$ ,  $\mu_{\text{O2}} = 0.03 \mu_B$ ,  $\mu_{\text{O3}} = 0.03 \mu_B$  and  $\mu_{\text{O4}} = -0.05 \mu_B$ . The sign of the Cu1 and O3 moments are the same, as are the Cu2 and O3 moments, driven by the fact that the short bonds are between these ions. The O2 moment is significantly larger than O1, consistent with the fact O1 forms a long bond with Cu1, but O2 forms a medium bond with Cu2 (which in turn couples their two moments).

The spin density (Fig. 5) illustrates the two dimensional nature of the electronic structure. The shape of this density clearly reflects the  $d_{x^2-y^2}$  orbital character around the Cu ions, with the lobes of the  $d$ -orbitals being directed along the short and medium Cu-O bonds (the medium one being out of plane for Cu2), giving rise to a direct overlap of the Cu- $d$  states with O- $p$  states of the neighboring oxygen ions. Since the Cu-O-Cu bond angles

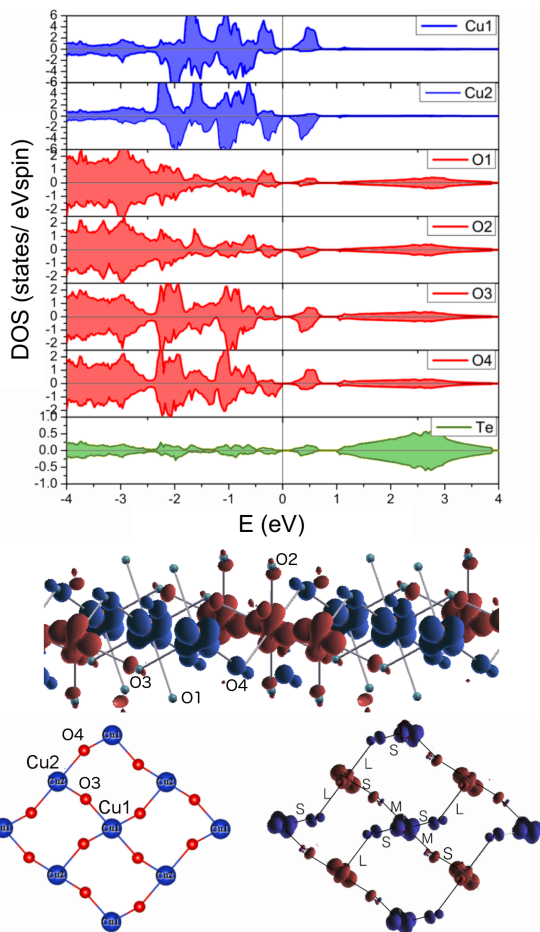


FIG. 5. Top panel: Atom resolved DOS for AFM  $\text{CuTeO}_4$ , showing a small gap within the hybridized Cu- $d$ , O- $p$  manifold of states. The positive and negative values on the y-axis are for spin-up and spin-down, respectively. Middle panel: Three-dimensional plot of the spin density in one of the Cu-O planes in the AFM state, with an isosurface at  $0.1 \text{ e}^-/\text{\AA}^3$ . Different colors represent the spin-up (spin-down) density. Bottom panel: view of the spin density in the  $\text{CuO}_2$  planes, with short, medium, and long Cu-O bonds indicated (S, M, L).

are much larger than  $90^\circ$ , one expects antiferromagnetic coupling, as we find, which is weaker than that in a typical cuprate which exhibits  $180^\circ$  bond angles. Interestingly, the magnetism is essentially two-dimensional, and not chain-like, despite the fact that structurally, the material is composed of S-M chains along the  $(1,0,1)$  planar directions, and S-L chains along the  $(1,0,-1)$  directions. The coupling of states from one plane to the next proceeds via the Te ions, but this only has a minor effect on the spin density. Structural relaxations do not affect the electronic structure significantly.

Given the similarities of the predicted electronic

structure of  $\text{CuTeO}_4$  to typical cuprates as well as the prediction of a magnetic ground state in the stoichiometric material, one might expect that a suitably doped phase would be a superconductor, which would be of significant interest given the very different Cu-O-Cu bond angles in this material (with values more reminiscent of materials with triangular lattices like herbertsmithite [18] than the  $180^\circ$  value found in an ideal cuprate). In this context, the magnetic wave vector ( $2Y$  in the notation of Fig. 1) couples the Fermi surfaces to one another in Fig. 3 (it is a reciprocal lattice vector). For the  $d_{x^2-y^2}$  superconducting state in a cuprate, one would have line nodes on the lower two surfaces in Fig. 3, whereas a  $d_{xy}$  state would have its nodes on the upper two. Since a number of copper tellurates have analogues where  $\text{Te}^{6+}$  is replaced by  $\text{Sb}^{5+}$ , hole doping of this material is a realistic possibility.

This work was supported by the Center for Emergent Superconductivity, an Energy Frontier Research Center funded by the US DOE, Office of Science, under Award No. DE-AC0298CH1088. We acknowledge the computing resources provided on Blues and Fusion, the high-performance computing clusters operated by the Laboratory Computing Resource Center at Argonne National Laboratory.

- 
- [1] B. Keimer, S. A. Kivelson, M. R. Norman, S. Uchida, and J. Zaanen, *Nature* **518**, 179 (2015).
  - [2] A. G. Christy, S. J. Mills, and A. R. Kampf, *Mineralogical Magazine* **80**, 415 (2016).
  - [3] L. Falck, O. Lindqvist, W. Mark, E. Philippot, and J. Moret, *Acta Crystallogr.* **B34**, 1450 (1978).
  - [4] L. Falck, O. Lindqvist, and J. Moret, *Acta Crystallogr.* **B34**, 896 (1978).
  - [5] D. Reinen and H. Weitzel, *Z. Anorg. Allg. Chem.* **424**, 31 (1976).
  - [6] P. Koehl and D. Reinen, *Z. Anorg. Allg. Chem.* **409**, 257 (1974).
  - [7] W. Klein, J. Curda, and M. Jansen, *Z. Anorg. Allg. Chem.* **633**, 231 (2007).
  - [8] J. Xu, A. Assoud, N. Soheilnia, S. Derakhshan, H. Cuthbert, J. Greedan, M. Whangbo, and H. Kleinke, *Inorg. Chem.* **44**, 5042 (2005).
  - [9] G. G. Gospodinov, *J. Mater. Sci. Lett.* **11**, 1460 (1992).
  - [10] P. Hohenberg and W. Kohn, *Phys. Rev.* **136**, B864 (1964).
  - [11] R. O. Jones and O. Gunnarsson, *Rev. Mod. Phys.* **61**, 689 (1989).
  - [12] P. Blaha, K. Schwarz, G. K. H. Madsen, D. Kvasnicka, and J. Luitz, *WIEN2k, An Augmented Plane Wave Plus Local Orbitals Program for Calculating Crystal Properties.*, Vienna University of Technology, Austria (2001).

- [13] E. Sjöstedt, L. Nördstrom, and D. Singh, *Solid State Commun.* **114**, 15 (2000).
- [14] J. P. Perdew, K. Burke, and M. Ernzerhof, *Phys. Rev. Lett.* **77**, 3865 (1996).
- [15] See Supplemental Material for results that include the spin orbit coupling and the Coulomb repulsion,  $U$ .
- [16] P. C. Burns, and F. C. Hawthorne, *Can. Miner.* **34**, 1089 (1996).
- [17] W. E. Pickett, *Rev. Mod. Phys.* **61**, 433 (1989).
- [18] M. P. Shores, E. A. Nytko, B. M. Bartlett, and D. G. Nocera, *J. Am. Chem. Soc.* **127**, 13462 (2005).